Solar Energy 184 (2019) 52–58

Contents lists available at ScienceDirect

Solar Energy

journal homepage: www.elsevier.com/locate/solener

Evaluation of impedance spectroscopy as a tool to characterize degradation mechanisms in silicon photovoltaics

Travis Yeow[a,b], Jing Sun[c], Zheng Yao[c], Jean-Nicolas Jaubert[c], Kevin P. Musselman[a,b]

[a] Department of Mechanical and Mechatronics Engineering, University of Waterloo, Waterloo, Ontario, Canada
[b] Waterloo Institute for Nanotechnology, University of Waterloo, Waterloo, Ontario, Canada
[c] Canadian Solar Inc., Guelph, Ontario, Canada

ARTICLE INFO

Keywords:
Impedance spectroscopy
Current induced degradation
Potential induced degradation
PERC
Bifacial module
Current induced regeneration

ABSTRACT

Advancements in photovoltaic technologies are hindered by degradation mechanisms such as potential induced degradation (PID) and current-induced degradation (CID). In this work, impedance spectroscopy is used to examine passivated emitter and rear cell (PERC) silicon modules with PID and CID. A comparison between control and degraded modules is done to identify key differences in the impedance spectra and determine the extent of the degradation. PID was observed at the module level as a dramatic reduction in shunt resistance, with a small amount of spatial inhomogeneity present in the degradation. It was found that accurate characterization of CID via measurement of the minority carrier lifetime requires a high bias voltage at the module level that exceeds the capabilities of a standard impedance spectrometer. Because of this, CID was also examined at the cell level, where reductions in minority carrier lifetimes could be accurately measured. A correlation between the reduction in minority carrier lifetime due to CID and a reduction in the power conversion efficiency was observed. Thus the PID and CID mechanisms studied here induce unique changes in the impedance spectroscopy results, making them distinguishable and quantifiable. Finally, the ability to mitigate CID through the use of different silicon wafers and a current induced regeneration process was characterized by impedance spectroscopy.

1. Introduction

Passivated emitter and rear cell (PERC) and bifacial double-glass modules are commercially-important architectures for silicon photovoltaics (PV). These photovoltaics are subject to degradation mechanisms such as current-induced degradation (CID) and potential induced degradation (PID) (Lancaster, 1989; Lindner et al., 2015; Nicolai et al., 2016; Oprea et al., 2016), which can result in significant reductions in the power conversion efficiency (PCE) (Chan et al., 2016). This degradation must therefore be reliably identified and addressed to ensure a suitably long lifetime for the PV modules.

Current techniques to characterize degradation include electroluminescence (EL) and photoluminescence (PL) tests, photoconductance lifetime tests, and current-voltage measurements, among others (Chan et al., 2016; Lindner et al., 2015; Oprea et al., 2016; Sharifi-Asl and Macdonald, 2014). Although the current methods are useful, individually they do not provide all information required to distinguish and quantitatively analyze degradation in a solar cell. Impedance spectroscopy is a non-destructive technique that has the potential to quantitatively analyze multiple aspects of a silicon photovoltaic's operation. By applying an AC signal of varying frequency over an electrical system, the real and imaginary impedances can be measured. These impedances are fit to an equivalent circuit that corresponds to physical features of a solar cell or module (Mora-Seró et al., 2009, 2008).

Impedance spectroscopy has been primarily used in other technologies, such as dye-sensitized, organic and perovskite photovoltaics, due to the resulting impedance spectra showing multiple arcs, which each correspond to a different physical process (Fabregat-Santiago et al., 2005; Guerrero et al., 2016; Guerrero and Garcia-Belmonte, 2017; Gupta et al., 2019; Musselman et al., 2011). For instance, in perovskite PV the ionic and electronic effects were decoupled to determine the ionic conductivity (Peng et al., 2018) similar to batteries (Haro et al., 2014). With silicon PV, each process happens simultaneously, resulting in a single arc in the impedance spectra (Mora-Seró et al., 2009), such that less information is typically revealed. Impedance spectroscopy has been used to characterize the series resistance (R_s), parallel resistance (R_p) and capacitance (C_p) of silicon solar cells under different illumination intensities and temperatures (Garland et al., 2011; Kumar et al., 2009; Mora-Seró et al., 2009; Yadav et al., 2015b). These values can

E-mail address: kevin.musselman@uwaterloo.ca (K.P. Musselman).

https://doi.org/10.1016/j.solener.2019.03.088
Received 24 December 2018; Received in revised form 25 March 2019; Accepted 26 March 2019
Available online 30 March 2019

translate to the series and shunt resistances, and minority carrier lifetime of the solar cell, which can be used to characterize its quality.

A more promising application for impedance spectroscopy in silicon PV may be as a diagnostic tool to evaluate different degradation mechanisms, which may induce changes in the measured impedance response. Impedance spectroscopy has been used to characterize corrosion of electrodes in silicon solar cells (Tanahashi et al., 2018) and defect activation energy/concentration (Sakakura et al., 2016) and depletion layer defects around the pn interface (Hayashi et al., 2012) in $Cu(In,Ga)Se_2$ (CIGS)-based solar cells. Notably, corrosion of the electrodes introduced another arc in the impedance spectrum, corresponding to a new time constant (Tanahashi et al., 2018). Oprea et al. used impedance spectroscopy to study PID in c-Si PV modules in which PID caused a dramatic reduction in the measured shunt resistance (Oprea et al., 2016). Shunting-type PID (PID-s) was assumed in their case, where it is suspected that shunt paths are created by the formation of stacking faults at the SiN_x/Si interface and the migration of Na^+ ions towards the stacking faults under the influence of a high electric field (Hacke et al., 2011; Luo et al., 2017a, 2017b; Oprea et al., 2016). A different PID mechanism (PID-p) has been reported for bifacial PERC modules, but to our knowledge, has not been characterized with impedance spectroscopy. In PID-p, surface polarization of the cell's rear surface causes positive charges to migrate towards the AlO_x/SiN_x layer diminishing the field passivation effect of this layer. It is induced by applying a large negative bias voltage at an elevated temperature. Increasing the negative bias and or temperature accelerates PID-p (Luo et al., 2017b; Pingel et al., 2010) and PID-p results in recombination along the rear surface of the module (Liang et al., 2018; Luo et al., 2017b). CID in Si solar cells or modules has not been examined by impedance spectroscopy but a reduction in minority carrier lifetimes is typically reported for CID (Nicolai et al., 2016; Sharifi-Asl and Macdonald, 2014), which should be observable with impedance spectroscopy. CID is commonly attributed to the formation of boron-oxygen complexes. Within the silicon, energy released from minority carriers during recombination activates the diffusion of oxygen, which migrates towards substitutional boron forming a metastable B-O defect. These defects act as recombination centers, which reduce the minority carrier lifetime (Chan et al., 2016; Hallam et al., 2013; Nicolai et al., 2016). Current and elevated temperature stresses have been known to induce CID (Chan et al., 2016; Lancaster, 1989; Pingel et al., 2010). Thus, while some preliminary work has been performed, the ability of impedance spectroscopy to distinguish and quantify different degradation mechanisms in Si photovoltaics has not been thoroughly assessed.

In this work, impedance spectroscopy is used to examine bifacial monocrystalline PERC modules in which PID-p was observed and standard (not bifacial) polycrystalline PERC modules and cells in which CID was observed. Comparisons between control and degraded modules and cells are done to identify key differences and determine the extent of degradation. We find that the PID and CID examined in this study induce unique changes in the impedance spectra, making them distinguishable and quantifiable. Notably, the PID modules show a reduction in shunt resistance at low forward biases and the CID cells show a reduction in minority carrier lifetime. Different batches of cells are measured to study the effect of different processing parameters on the resulting CID, as characterized by impedance spectroscopy.

2. Experimental

2.1. Silicon modules and cells

Special PID sensitive double-glass bifacial silicon modules consisting of monocrystalline p-type passivated emitter and rear cell (PERC) cells encapsulated using Ethylene Vinyl Acetate (EVA) polymer were provided by Canadian Solar Inc. Both a control module and a PID-degraded module were examined by impedance spectroscopy. The degraded module had been subjected to −1500 V at 85 °C and 85% humidity for 96 h. This resulted in a P_{max} degradation of 37% for backside illumination and 6% for frontside illumination, where P_{max} is the maximum output power, as seen in Table S1 of the Supplementary Information. Standard (not bifacial) polycrystalline PERC modules were also provided by Canadian Solar Inc. A control module was again provided, along with a CID-degraded module. CID degradation had been induced by applying a current of about 0.5 A (the difference between the short circuit current, I_{SC}, and the current at maximum power, I_{MP}) at 85 °C for 200 h. This resulted in a P_{max} degradation of 2%, as seen in Table S2 of the Supplementary Information. Polycrystalline PERC cells were prepared by Canadian Solar Inc. using two different types of p-type silicon, which were expected to have different levels of quality. Some of the cells underwent a current induced regeneration (CIR) process prior to CID conditioning. CID was induced in half of the cells using slightly different conditioning than for the modules (3.5 A at 100 °C for 4 h). A summary of the cell properties and quantity tested is provided in Table 1.

Table 1
PERC cells provided by Canadian Solar Inc.

Cell properties	Number of control cells	Number of cells after CID conditioning
High quality silicon (no CIR)	10	10
Lower quality silicon (no CIR)	15	15
High quality silicon + CIR		
Batch 1	15	15
Batch 2	10	10

2.2. Impedance spectroscopy measurements

A Gamry Interface 1000E potentiostat was used to measure the impedance of the solar modules and solar cells at room temperature. Frequencies applied were 100 kHz to 1 Hz with 10 measurements taken every decade. Above 100 kHz, the impedance of the connectors and lead wires dominate and invalidate assumptions for fitting (Mora-Seró et al., 2009; Oprea et al., 2016). All measurements were carried out in the dark (Garland et al., 2011; Kumar et al., 2005; Lindner et al., 2015), as heating of the cells during prolonged impedance measurements and the short exposure time of standard flash testers make measurement under illumination difficult. The resulting data was analyzed using Gamry Echem Analyst. Nyquist plots were fit to an equivalent circuit with a series resistor and a resistor in parallel with a capacitor or a constant phase element. Goodness of fit was calculated by the Gamry software using the Simplex method.

2.3. Photovoltaic characterization

The current-voltage curves and power conversion efficiency of individual cells and modules were measured using a Sinton FCT-450 and a PASAN SunSim 3C (class AAA simulator), respectively. The bifacial monocrystalline PERC modules were measured by alternatively obstructing the front and rear side with a low reflectivity cover. All measurements were carried out at 1 sun, with equipment being calibrated using a standard reference cell and a primary reference module for the cell and module measurements, respectively. BT Imaging R3 equipment was used to characterize the electroluminescence of the solar cells. For EL measurements, a current of 3.5 A was used.

3. Results

3.1. PID in modules

Fig. 1a shows the Nyquist plots for the double-glass monocrystalline bifacial silicon modules with and without PID for a DC bias of 5 V applied across the 72 cells in series, resulting in a bias of approximately

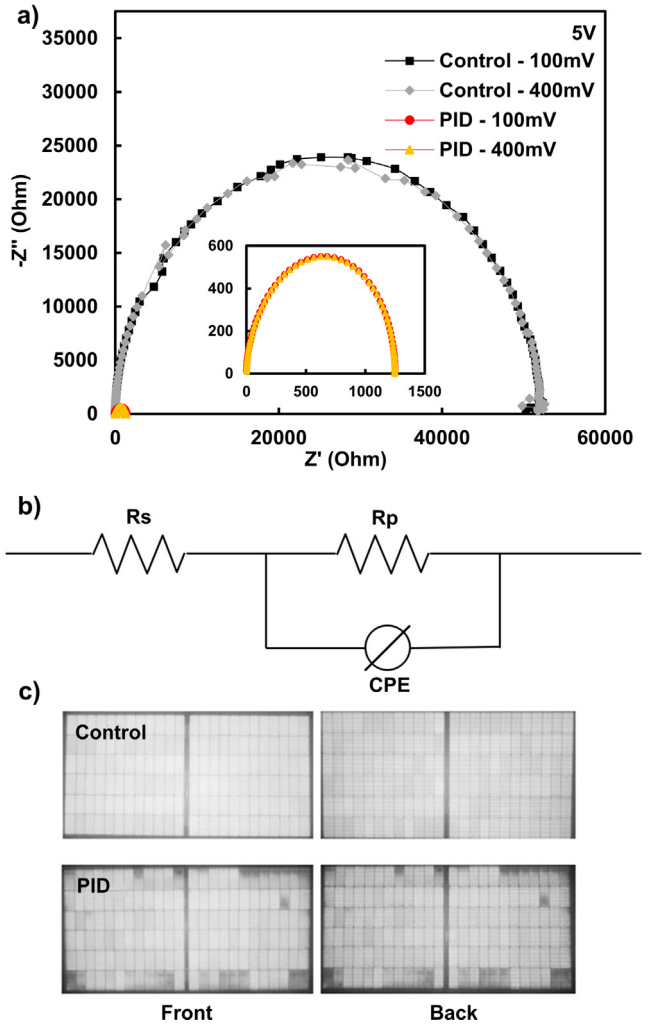

Fig. 1. Characterization of bifacial modules with and without PID. (a) Nyquist plots of the bifacial modules measured at a 5 V bias using 100 mV and 400 mV AC voltages. (b) Equivalent circuit used to fit the Nyquist plots. (c) Electroluminescence measurements of the control and PID-degraded modules from the front and back.

0.07 V per cell. AC voltages of 100 mV and 400 mV were applied and were found to result in identical spectra. A reduction in the parallel resistance (width of the semicircle in the Nyquist plot) of more than 1 order of magnitude is observed for the PID-degraded module. The parallel resistance is a combination of the dynamic diode and shunt resistances. Under increasing forward bias, the dynamic diode resistance is known to decrease to negligible values (Chenvidhya et al., 2005; Kumar et al., 2005; Suresh, 1996), such that the parallel resistance is equivalent to the dynamic diode resistance. When the bias voltage is close to zero or reverse biased, the diode resistance is expected to be much greater than the shunt resistance, making the parallel resistance equivalent to the shunt resistance (Chenvidhya et al., 2005). Ideally a reverse bias would be applied to the modules to isolate the shunt resistances, but this was not possible due to reverse-polarity-protection, which prevents reverse voltages from damaging the circuit (Chowdhury and Mourshed, 2016; Wills et al., 1996). Instead, the DC voltage was kept low to limit the impact of the dynamic diode resistance, such that the measured parallel resistance should approximate the shunt resistance. A plot of R_p versus bias voltage for some of the individual PERC cells is included in Fig. S1 and shows that the parallel resistance only started to decrease significantly (indicating the influence of the dynamic diode resistance) when the cell voltage was greater than 0.1 V. Hence, at a 5 V bias (0.07 V per cell), the parallel resistance is expected to closely approximate the shunt resistance.

The Nyquist plots were fit to an equivalent circuit with a constant phase element (CPE), as shown in Fig. 1b, which provided a better fit than a circuit with a simple capacitor. A constant phase element is typically used when the Nyquist plot deviates from a perfect semicircle due to inhomogeneity in the circuit and is associated with traps and defects (Hsu and Mansfeld, 2001; Kane et al., 2016; Longo et al., 2002). The elements of a CPE include Q and ϕ, as given in Eq. (1).

$$Z = \frac{1}{(Q\omega i)^{\phi}} \tag{1}$$

ϕ is a value between 0 and 1, where 1 corresponds to the element being an ideal capacitor and 0 being a resistor. Q is the capacitance when $\phi \approx 1$. Table 2 lists the equivalent circuit parameters obtained for the bifacial modules at the two AC voltages. The fitted parallel resistance R_p, drops significantly from approximately 51 kΩ in the control module to 1.2 kΩ in the module with PID, consistent with the Nyquist plot in Fig. 1a. The series resistance remains very small, suggesting that significant contact degradation does not occur (Correa-Baena et al., 2017; Mora-Seró et al., 2009; Tanahashi et al., 2018). It is seen that ϕ is 0.996 for the control module and 0.960 for the PID module. This indicates uniformity within a cell and from cell-to-cell in the circuit for the control module and slight inhomogeneity for the PID module. Since $\phi > 0.95$ the spatial inhomogeneity can be considered relatively small (Irvine et al., 2009). The inhomogeneity is confirmed in EL test results seen in Fig. 1c. In an EL test, a current is passed through a solar cell or module and radiative recombination of the injected carriers causes light emission, which is measured by a detector. Uniform light emission would be expected from the surface of a homogeneous cell or module, whereas defects appear darker because they dissipate power via non-radiative recombination and hence reveal positions of inhomogeneity (Fuyuki and Kitiyanan, 2009; Haunschild et al., 2009; Kojima et al., 2011). It is seen in Fig. 1c that the cells in the PID-degraded module show more darkening, particularly around the edges of the module. However, within the cells there does not appear to be significant localized areas of darkening. Hence the decrease in ϕ can be attributed to a non-uniform degradation across the module, where the cells along the edges experience greater PID.

Overall, there is a P_{max} loss of approximately 37% (for backside illumination) and a loss in shunt resistance of more than 1 order of magnitude (as measured by impedance spectroscopy) in the PID-degraded bifacial module. Oprea et al. previously reported a larger P_{max} loss of approximately 70% for c-Si modules experiencing PID and similarly observed a larger drop in shunt resistance of 3 orders of magnitude by impedance spectroscopy (measured using a 2 V bias and 2 V AC signal) (Oprea et al., 2016). It is noted that in the modules measured by Oprea et al., the P_{max} loss was mainly due to a reduced fill factor and

Table 2
Equivalent circuit parameters for one bifacial module with PID and one without PID (at 5 V bias).

	R_s (Ω)	R_p (Ω)	Q (F)	ϕ	Goodness of fit
Bifacial Control 100 mV	1.16E−07	5.15E+04	1.37E−07	0.996	3.12E−03
Bifacial Control 400 mV	2.66E−06	5.06E+04	1.38E−07	0.996	3.93E−03
Bifacial PID 100 mV	1.07E−06	1.24E+03	2.13E−07	0.960	2.30E−03
Bifacial PID 400 mV	1.07E−06	1.24E+03	2.13E−07	0.960	2.30E−03

open-circuit voltage. They attributed the PID to Na^+ diffusion into stacking faults (PID-s). Although they used a simple capacitor in the equivalent circuit, PID-s defects are expected to result in significant inhomogeneity due to localized shunt pathways in the cell (Luo et al., 2017b; Naumann et al., 2014), such that a constant phase element may have been more suitable (goodness of fits were not provided). In the PID-degraded module measured here, the P_{max} loss was mainly due to a reduced fill factor and short circuit current (current-voltage measurements are included in Table S1 and Fig. S2 in the Supplementary Information), consistent with PID caused by a deterioration of the field passivation effect (PID-p). It has been reported that the cell fill factor is only moderately affected by PID-p, whereas the module fill factor decreases significantly due to PID-p, which was attributed to mismatch between the various degraded cells in the module (Khoo et al., 2017; Liang et al., 2018). PID-p has been reported to produce homogenous cell degradation related to increased surface recombination (Liang et al., 2018; Luo et al., 2017b; Naumann et al., 2014). This is consistent with the lack of localized defects observed within the cells in the EL measurements in Fig. 1c, and the modest deviation of the CPE parameter ϕ from 0.996 to 0.960 in the module's equivalent circuit. Thus impedance spectroscopy may not only allow identification and quantification of PID via a reduction in the shunt resistance, but may also permit different modes of PID to be distinguished (e.g., an equivalent circuit with a CPE may show a distinction between PID-s and PID-p in modules based on the CPE parameters). Study of modules with a wider variety of PID conditions can be pursued in the future to confirm this.

3.2. CID in modules

Fig. 2a shows the Nyquist plots for the polycrystalline PERC modules with and without CID, again at a DC bias of 5 V. As before, similar results were obtained using 100 mV and 400 mV AC voltages. In contrast to the PID-degraded monocrystalline bifacial module, in which a large reduction in shunt resistance was observed, a slight increase in shunt resistance is observed for the CID-degraded PERC module. This is unexpected as the shunt resistance is expected to decrease under CID (Pingel et al., 2010; Sopori et al., 2012). However, the shunt resistance only increases by approximately 12%, as compared to the more than an order of magnitude reduction in shunt resistance observed in the PID module, such that this increase in R_p is attributed to variability amongst the cells and modules, rather than the current-induced degradation. This is supported by Fig. S1 of the Supporting Information, where it is seen that at bias voltages near zero, the R_p of individual control and CID polycrystalline PERC cells varies, with some CID cells having a larger R_p than the control cells. As the bias voltage increases, the R_p dips to expected values and is lower in the CID cells than the control cells. Others have similarly reported that due to the sensitive nature of impedance spectroscopy, a significant impedance variability can be found within batches of modules and cells (Johnson et al., 2011; Moehlecke and Zanesco, 2012; Pingel et al., 2010; Sopori et al., 1999).

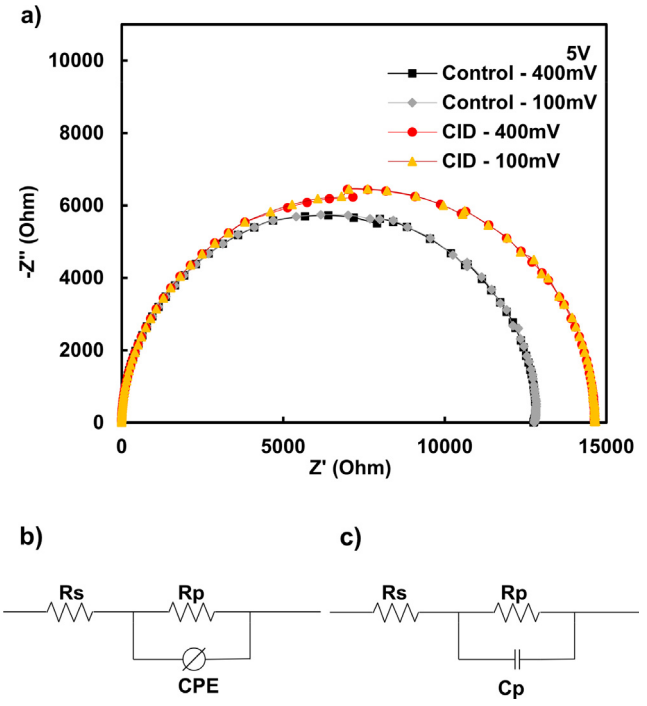

Fig. 2. Characterization of PERC modules with and without CID. (a) Nyquist plots of PERC modules measured at a 5 V bias using 100 mV and 400 mV AC voltages. (b and c) Equivalent circuits used to fit the Nyquist plots with a constant phase element and a capacitor respectively.

The Nyquist plots were again fit to a circuit with a constant phase element, as shown in Fig. 2b, and the obtained equivalent circuit parameters are found in Table 3. As for the case of PID in the bifacial modules discussed in Section 3.1, an increase in the series resistance was not observed for CID in the standard PERC modules. Unlike for the bifacial modules, it is seen in Table 3 that ϕ is very close to 1 for both PERC modules (with and without CID). Hence the PERC modules can be accurately fit to an equivalent circuit with a capacitor instead of a constant phase element, as shown in Fig. 2c and Table 3. Fitting to a capacitor C_p facilitates the analysis of CID because a reduction in minority carrier lifetime is expected for CID, which can be measured by examining the time constant of the Nyquist plot (Nicolai et al., 2016; Sharifi-Asl and Macdonald, 2014). The time constant can be determined by the equation:

$$\tau = R_p C_p \quad (2)$$

This is the parallel capacitance multiplied by the parallel resistance and corresponds to the time a carrier exists in an excited state in a cell after electron-hole generation before recombining (Mora-Seró et al., 2009). As indicated in the lower portion of Table 3, the module-level time constants obtained for the CID-degraded module in Fig. 2 were actually slightly larger than those obtained for the control module. Since these measurements were performed at a 5 V forward bias, a bias of only approximately 0.07 V was applied to each of the 72 cells in series. As will be discussed in Section 3.3, the minority carrier lifetime in the PERC cells cannot be accurately measured at this bias. Higher bias voltages of about 0.5 V per cell are required. In this bias range, the space charge region recombination and quasi-neutral region recombination are both present and the combined influence of both mechanisms on the carrier lifetime is maximized (Yadav et al., 2015a). Therefore, it was identified that to accurately identify CID in silicon modules, an impedance spectrometer capable of applying larger bias voltages (e.g., greater than 40 V) would be required for further investigation. It is noted that while common impedance spectrometers are not capable of such high bias voltages, some manufacturers do produce models that can produce biases in this range.

3.3. CID in cells

To assess the ability of impedance spectroscopy to identify and quantify CID, polycrystalline PERC cells were studied, as a suitably large bias voltage could be applied with the standard spectrometer used. The cells that were made from high quality silicon and did not undergo CIR were measured at bias voltages ranging from −0.4 V to 0.6 V using an AC voltage of 10 mV. The resulting Nyquist plots were fit well using an equivalent circuit consisting of a series resistor, parallel resistor, and parallel capacitor. The time constants obtained from the equivalent circuits were plotted as a function of bias voltage, as shown in Fig. 3. At lower bias voltages, the time constant is relatively constant. The space charge region (SCR) recombination dominates at low forward and reverse biases (−0.4 to 0.35 V). As the forward bias increases, the

Table 3
Equivalent circuit parameters for one PERC module with CID and one without CID obtained by fitting equivalent circuits with a CPE or a capacitor (at 5 V bias).

CPE	Rs (Ω)	Rp (Ω)	Q (F)	Φ	Goodness of fit
PERC Control 100 mV	6.15E−06	1.26E+04	1.68E−07	0.992	2.28E−03
PERC Control 400 mV	2.11E−06	1.26E+04	1.67E−07	0.993	2.28E−03
PERC CID 100 mV	1.01E−01	1.43E+04	2.02E−07	0.988	4.09E−03
PERC CID 400 mV	1.27E−01	1.43E+04	1.99E−07	0.989	4.16E−03
Capacitor	Rs (Ω)	Rp (Ω)	Cp (F)	Time const. (s)	Goodness of fit
PERC Control 100 mV	3.77E−01	1.26E+04	1.56E−07	1.95E−03	2.45E−03
PERC Control 400 mV	1.28E−03	1.26E+04	1.55E−07	1.95E−03	2.48E−03
PERC CID 100 mV	3.93E−01	1.42E+04	1.80E−07	2.56E−03	4.64E−03
PERC CID 400 mV	5.97E−07	1.42E+04	1.79E−07	2.55E−03	4.70E−03

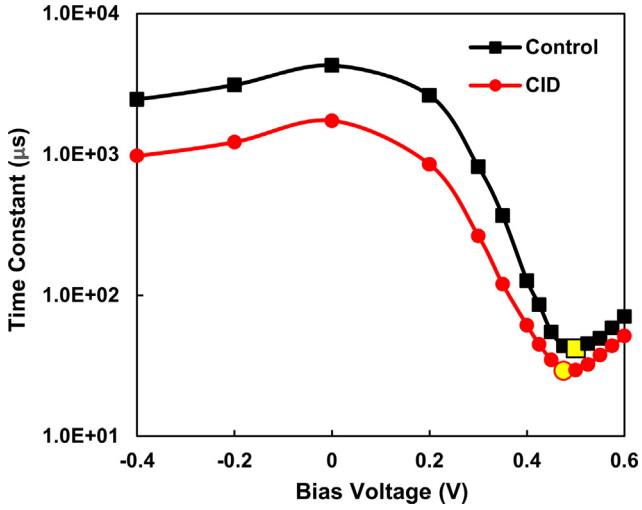

Fig. 3. Time constant as a function of bias voltage for high quality silicon PERC cells (with no CIR), with and without CID conditioning.

involvement of shunt resistance increases causing the time constant to decline. The bias voltage increases to a zone where the SCR and quasi-neutral region (QNR) recombination are both present causing the time constant to further decrease (0.35–0.55 V) (Yadav et al., 2015a). Under the maximum effect of SCR and QNR recombination, the time constant reaches a minimum where the minority carrier lifetime can be obtained (Yadav et al., 2015a). This is seen to occur at a bias voltage of approximately 0.5 V in Fig. 3 and can vary from cell to cell. Thus, minority carrier lifetimes of 29 µs and 42 µs are obtained from Fig. 3 for the cells with and without CID, respectively.

The minority carrier lifetimes of all 100 PERC cells were measured in a similar manner, and a clear relationship was observed with the measured PCEs. In Fig. 4, the lifetimes of the batches of cells with varying pre-treatments are shown as a function of their PCE. These plots clearly illustrate the effects of CID. CID cells are clustered in the bottom left of the plots, corresponding to lower PCE and minority carrier lifetime values, whereas the cells that did not undergo CID conditioning are located in the upper right, with higher PCEs and lifetimes. This suggests that impedance spectroscopy can provide a quantitative measure of the degree of CID (in terms of the reduction in minority carrier lifetime) within a batch of solar cells.

To compare the effectiveness of different CID mitigation strategies, the percent reductions in average PCEs and minority carrier lifetimes resulting from CID conditioning are compared for different cell batches in Table 4. The percent decreases in average minority carrier lifetimes and average PCEs resulting from CID conditioning were large for batches where CIR was not employed. That is, 16.72% and 19.26% decreases in average lifetime and 1.62% and 1.78% decreases in average PCE were observed for the lower quality Si (no CIR) and high quality silicon (no CIR) batches, respectively. It should be noted that the decreases were smaller than expected in batches where the silicon was expected to be of lower quality. This suggests that the quality may not be inferior or this silicon is less susceptible to CID. The smallest percent decreases are observed in batch 1 of the cells that used high quality silicon and CIR. This batch demonstrated a 12.21% decrease in average minority carrier lifetime and a 1.35% decrease in PCE. These results suggest that CIR is an effective process in reducing CID in the polycrystalline PERC cells.

Interestingly, the other high quality silicon and CIR batch (batch 2) showed a larger decrease in average minority carrier lifetime (18.53%) but a similar decrease in average PCE (1.34%) when compared to batch 1. This indicates that while a relation between PCE and minority carrier lifetime can be observed within a batch of cells (as shown in Fig. 4), the relationship between % reduction in average PCE and % reduction in lifetime resulting from CID may vary from batch to batch. This is likely due to parameters other than those considered here (type of silicon, use of CIR treatment) influencing the cells' response to CID conditioning (Johnson et al., 2011; Moehlecke and Zanesco, 2012; Pingel et al., 2010; Sopori et al., 1999).

4. Conclusions

Impedance spectroscopy is a powerful tool with capabilities yet to be fully exploited in the field of silicon photovoltaics. Here it was used to distinguish and quantify PID-p and CID in silicon solar modules and cells. PID-p in double glass bifacial modules was characterized by a dramatic reduction in shunt resistance. Comparison to a previous report on PID-s indicates that larger reductions in shunt resistance correspond to more degradation. While other techniques, such as IV measurements, can be used to measure the shunt resistance, by fitting the impedance spectroscopy data to an equivalent circuit with a constant phase element, this technique also provides a measure of the degree of inhomogeneity within the module (as indicated by the constant phase element parameter ϕ), which has the potential to distinguish between PID-p and PID-s.

CID was characterized by examining the minority carrier lifetime of cells due to the high bias voltages required to probe the minority carrier lifetime in a module. A correlation between PCE and minority carrier lifetime was observed, with a lower lifetime due to CID resulting in a lower PCE. CID did not affect the shunt resistance significantly, such that CID and PID are distinguishable by impedance spectroscopy. The influence of different silicon wafers and a current-induced regeneration process on the extent of CID in the PERC cells was characterized. While the CIR process was found to reduce the amount of CID, the use of what was expected to be lower quality silicon wafers did not lead to a clear reduction in the minority carrier lifetimes.

Overall, impedance spectroscopy appears to be a promising method for characterising degradation mechanisms in solar cell modules. In particular, it is well suited for non-destructive measurements in the field and in factory settings. To further clarify its abilities, the methodology demonstrated here can be applied to solar cells and modules displaying a wider variety of degradation mechanisms of varying

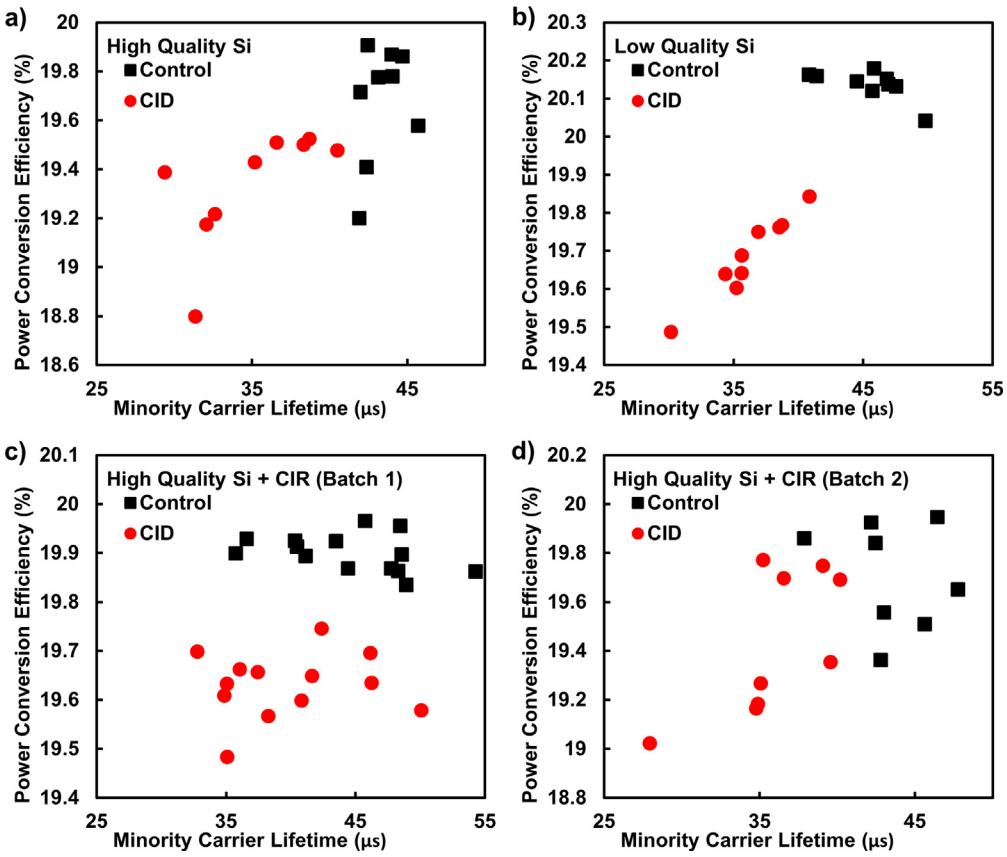

Fig. 4. Minority carrier lifetime as a function of power conversion efficiency for batches of varying pre-treatments: (a) high quality Si (no CIR), (b) lower quality Si (no CIR), (c) high quality Si + CIR (batch 1), (d) high quality Si + CIR (batch 2).

Table 4
Lifetime and PCEs of PERC cells with and without CID conditioning.

Cell properties	Number of cells	CID conditioning	Lifetime (μs)	% Decrease lifetime due to CID	PCE (%)	% Decrease PCE due to CID
High quality Si (no CIR)	10	No	43.3 ± 1.4		19.68 ± 0.01	
High quality Si (no CIR)	10	Yes	35.0 ± 1.3	19.26%	19.33 ± 0.08	1.78%
Lower quality Si (no CIR)	15	No	43.0 ± 1.7		19.98 ± 0.02	
Lower quality Si (no CIR)	15	Yes	35.8 ± 0.9	16.72%	19.68 ± 0.03	1.62%
High quality Si + CIR (Batch 1)	15	No	45.3 ± 1.5		19.90 ± 0.01	
High quality Si + CIR (Batch 1)	15	Yes	39.8 ± 1.5	12.21%	19.63 ± 0.02	1.35%
High quality Si + CIR (Batch 2)	10	No	44.1 ± 1.1		19.69 ± 0.01	
High quality Si + CIR (Batch 2)	10	Yes	35.9 ± 1.2	18.53%	19.43±0.09	1.34%

degrees in the future.

Funding

This work was supported by the Natural Sciences and Engineering Research Council of Canada [grant number EGP 519751-2017]; the Ontario Research Fund – Research Infrastructure [project number 35552]; and the Canadian Foundation for Innovation John R. Evans Leaders Fund [project number 35552].

Appendix A. Supplementary material

Supplementary data to this article can be found online at https://doi.org/10.1016/j.solener.2019.03.088.

References

Chan, C.E., Payne, D.N.R., Hallam, B.J., Abbott, M.D., Fung, T.H., Wenham, A.M., Tjahjono, B.S., Wenham, S.R., 2016. Rapid stabilization of high-performance multicrystalline P-type silicon PERC cells. IEEE J. Photovolt. 6, 1473–1479. https://doi.org/10.1109/JPHOTOV.2016.2606704.

Chenvidhya, D., Kirtikara, K., Jivacate, C., 2005. PV module dynamic impedance and its voltage and frequency dependencies. Sol. Energy Mater. Sol. Cells 86, 243–251. https://doi.org/10.1016/j.solmat.2004.07.005.

Chowdhury, S.A., Mourshed, M., 2016. Off-grid electrification with solar home systems: an appraisal of the quality of components. Renew. Energy 97, 585–598. https://doi.org/10.1016/j.renene.2016.06.017.

Correa-Baena, J.P., Turren-Cruz, S.H., Tress, W., Hagfeldt, A., Aranda, C., Shooshtari, L., Bisquert, J., Guerrero, A., 2017. Changes from bulk to surface recombination mechanisms between pristine and cycled perovskite solar cells. ACS Energy Lett. 2, 681–688. https://doi.org/10.1021/acsenergylett.7b00059.

Fabregat-Santiago, F., Bisquert, J., Garcia-Belmonte, G., Boschloo, G., Hagfeldt, A., 2005. Influence of electrolyte in transport and recombination in dye-sensitized solar cells studied by impedance spectroscopy. Sol. Energy Mater. Sol. Cells 87, 117–131. https://doi.org/10.1016/j.solmat.2004.07.017.

Fuyuki, T., Kitiyanan, A., 2009. Photographic diagnosis of crystalline silicon solar cells utilizing electroluminescence. Appl. Phys. A Mater. Sci. Process. 96, 189–196. https://doi.org/10.1007/s00339-008-4986-0.

Garland, J.E., Crain, D.J., Roy, D., 2011. Impedance spectroscopy coupled with voltammetry for quantitative evaluation of temperature and voltage dependent parameters of a silicon solar cell. Sol. Energy 85, 2912–2923. https://doi.org/10.1016/j.solener.2011.08.029.

Guerrero, A., Garcia-Belmonte, G., 2017. Recent advances to understand morphology stability of organic photovoltaics. Nano-Micro Lett. 9. https://doi.org/10.1007/s40820-016-0107-3.

Guerrero, A., Garcia-Belmonte, G., Mora-Sero, I., Bisquert, J., Kang, Y.S., Jacobsson, T.J., Correa-Baena, J.P., Hagfeldt, A., 2016. Properties of contact and bulk impedances in hybrid lead halide perovskite solar cells including inductive loop elements. J. Phys. Chem. C 120, 8023–8032. https://doi.org/10.1021/acs.jpcc.6b01728.

Gupta, S.K., Pali, L.S., Garg, A., 2019. Impedance spectroscopy on degradation analysis of polymer/fullerene solar cells. Sol. Energy 178, 133–141. https://doi.org/10.1016/j.solener.2018.12.024.

Hacke, P., Terwilliger, K., Smith, R., Glick, S., Pankow, J., Kempe, M., Bennett, S.K.I., Kloos, M., 2011. System voltage potential-induced degradation mechanisms in PV modules and methods for test. In: Conf. Rec. IEEE Photovolt. Spec. Conf., pp. 000814–000820. doi:10.1109/PVSC.2011.6186079.

Hallam, B.J., Wenham, S.R., Hamer, P.G., Abbott, M.D., Sugianto, A., Chan, C.E., Wenham, A.M., Eadie, M.G., Xu, G.Q., 2013. Hydrogen passivation of B-O defects in Czochralski silicon. Energy Proc. 38, 561–570. https://doi.org/10.1016/j.egypro.2013.07.317.

Haro, M., Song, T., Guerrero, A., Bertoluzzi, L., Bisquert, J., Paik, U., Garcia-Belmonte, G., 2014. Germanium coating boosts lithium uptake in Si nanotube battery anodes. Phys. Chem. Chem. Phys. 16, 17930–17935. https://doi.org/10.1039/c4cp02377c.

Haunschild, J., Glatthaar, M., Kasemann, M., Rein, S., Weber, E.R., 2009. Fast series resistance imaging for silicon solar cells using electroluminescence. Phys. Status Solidi - Rapid Res. Lett. 3, 227–229. https://doi.org/10.1002/pssr.200903175.

Hayashi, M., Yamazaki, C., Sugiyama, M., Itagaki, M., Hamidon, N.B., Hirose, Y., 2012. Application of impedance spectroscopy to investigate the electrical properties around the pn interface of Cu(In, Ga)Se2 solar cells. Thin Solid Films 535, 287–290. https://doi.org/10.1016/j.tsf.2012.11.070.

Hsu, C.H., Mansfeld, F., 2001. Concernng the conversion of the constant phase element parameter Y0into a capacitance. Corrosion 57, 747–748. https://doi.org/10.5006/1.3280607.

Irvine, S.J.C., Garcia-Belmonte, G., Al Turkestani, M.K., Barrioz, V., Proskuryakov, Y.Y., Bisquert, J., Jones, E.W., Lamb, D., Fabregat-Santiago, F., Durose, K., Mora-Seró, I., 2009. Impedance spectroscopy of thin-film CdTe/CdS solar cells under varied illumination. J. Appl. Phys. 106, 044507. https://doi.org/10.1063/1.3204484.

Johnson, J., Schoenwald, D., Kuszmaul, S., Strauch, J., Bower, W., 2011. Creating dynamic equivalent PV circuit models with impedance. In: 37th IEEE Photovoltaic Specialists Conference, pp. 2328–2333.

Kane, S.N., Mishra, A., Dutta, A.K., 2016. Preface: international conference on recent trends in physics (ICRTP 2016). J. Phys. Conf. Ser. 755. https://doi.org/10.1088/1742-6596/755/1/011001.

Khoo, Y.S., Wang, Y., Luo, W., Ramakrishna, S., Wong, J.K.C., Singh, J.P., Aberle, A.G., 2017. Investigation of potential-induced degradation in n-PERT bifacial silicon photovoltaic modules with a glass/glass structure. IEEE J. Photovolt. 8, 16–22. https://doi.org/10.1109/jphotov.2017.2762587.

Kojima, O., Harada, Y., Hasegawa, A., Kita, T., Inoue, T., Hu, W., 2011. Intermediate band photovoltaics based on interband-intraband transitions using In0.53Ga0.47As/InP superlattice. Prog. Photovoltaics Res. Appl. https://doi.org/10.1002/pip.1208.

Kumar, R.A., Suresh, M.S., Nagaraju, J., 2005. Silicon (BSFR) solar cell AC parameters at different temperatures. Sol. Energy Mater. Sol. Cells 85, 397–406. https://doi.org/10.1016/j.solmat.2004.05.017.

Kumar, S., Singh, P.K., Chilana, G.S., 2009. Study of silicon solar cell at different intensities of illumination and wavelengths using impedance spectroscopy. Sol. Energy Mater. Sol. Cells 93, 1881–1884. https://doi.org/10.1016/j.solmat.2009.07.002.

Lancaster, M., 1989. Summary for policymakers. Clim. Chang. 2013 – Phys. Sci. Basis 53, 1–30. https://doi.org/10.1017/CBO9781107415324.004.

Liang, T.S., Terwilliger, K., Khoo, Y.S., Hacke, P., Aberle, A.G., Wang, Y., Luo, W., Ramakrishna, S., 2018. Elucidating potential-induced degradation in bifacial PERC silicon photovoltaic modules. Prog. Photovolt. Res. Appl. 26, 859–867. https://doi.org/10.1002/pip.3028.

Lindner, T., Bartzsch, M., Engelhart, P., Müller, J.W., Stenzel, F., Ploigt, H.-C., Szpeth, A., Petter, K., Heitmann, J., Kersten, F., Stekolnikov, A., 2015. Degradation of multicrystalline silicon solar cells and modules after illumination at elevated temperature. Sol. Energy Mater. Sol. Cells 142, 83–86. https://doi.org/10.1016/j.solmat.2015.06.015.

Longo, C., Nogueira, A.F., Paoli, M. De, 2002. Solid-state and flexible dye-sensitized TiO2 solar cells: a study by electrochemical impedance spectroscopy. J. Phys. Chem. B 106, 5925–5930. https://doi.org/10.1021/jp014456u.

Luo, W., Khoo, Y.S., Hacke, P., Naumann, V., Lausch, D., Harvey, S.P., Singh, J.P., Chai, J., Wang, Y., Aberle, A.G., Ramakrishna, S., 2017a. Potential-induced degradation in photovoltaic modules: a critical review. Energy Environ. Sci. 10, 43–68. https://doi.org/10.1039/c6ee02271e.

Luo, W., Khoo, Y.S., Singh, J.P., Wong, J.K.C., Wang, Y., Aberle, A.G., Ramakrishna, S., 2017b. Investigation of Potential-Induced Degradation in n-PERT Bifacial Silicon Photovoltaic Modules with a Glass/Glass Structure. IEEE J. Photovolt. 1–7. https://doi.org/10.1109/JPHOTOV.2017.2762587.

Moehlecke, A., Zanesco, I., 2012. Development of silicon solar cells and photovoltaic modules in Brazil: analysis of a pilot production. Mater. Res. 15, 581–588. https://doi.org/10.1590/s1516-14392012005000084.

Mora-Seró, I., Garcia-Belmonte, G., Boix, P.P., Vázquez, M.A., Bisquert, J., 2009. Impedance spectroscopy characterisation of highly efficient silicon solar cells under different light illumination intensities. Energy Environ. Sci. 2, 678–686. https://doi.org/10.1039/b812468j.

Mora-Seró, I., Luo, Y., Garcia-Belmonte, G., Bisquert, J., Muñoz, D., Voz, C., Puigdollers, J., Alcubilla, R., 2008. Recombination rates in heterojunction silicon solar cells analyzed by impedance spectroscopy at forward bias and under illumination. Sol. Energy Mater. Sol. Cells 92, 505–509. https://doi.org/10.1016/j.solmat.2007.11.005.

Musselman, K.P., Marin, A., Wisnet, A., Scheu, C., MacManus-Driscoll, J.L., Schmidt-Mende, L., 2011. A novel buffering technique for aqueous processing of zinc oxide nanostructures and interfaces, and corresponding improvement of electrodeposited ZnO-Cu2O photovoltaics. Adv. Funct. Mater. 21, 573–582. https://doi.org/10.1002/adfm.201001956.

Naumann, V., Geppert, T., Großer, S., Wichmann, D., Krokoszinski, H.J., Werner, M., Hagendorf, C., 2014. Potential-induced degradation at interdigitated back contact solar cells. Energy Proc. 55, 498–503. https://doi.org/10.1016/j.egypro.2014.08.015.

Nicolai, M., Zanuccoli, M., Galiazzo, M., Bertazzo, M., Sangiorgi, E., Fiegna, C., 2016. Simulation study of light-induced, current-induced degradation and recovery on PERC solar cells. Energy Proc. 92, 153–159. https://doi.org/10.1016/j.egypro.2016.07.014.

Oprea, M.I., Spataru, S. V., Sera, D., Poulsen, P.B., Thorsteinsson, S., Basu, R., Andersen, A.R., Frederiksen, K.H.B., 2016. Detection of potential induced degradation in c-Si PV panels using electrical impedance spectroscopy. In: 2016 IEEE 43rd Photovoltaic Specialists Conference (PVSC). IEEE, pp. 1575–1579. doi:10.1109/PVSC.2016.7749885.

Peng, W., Aranda, C., Bakr, O.M., Garcia-Belmonte, G., Bisquert, J., Guerrero, A., 2018. Quantification of ionic diffusion in lead halide perovskite single crystals. ACS Energy Lett. 3, 1477–1481. https://doi.org/10.1021/acsenergylett.8b00641.

Pingel, S., Koshnicharov, D., Frank, O., Geipel, T., Zemen, Y., Striner, B., Berghold, J., 2010. Initial degradation of industrial silicon solar cells in solar panels. In: Proc. 25th Eur. Photovolt. Sol. Energy Conf. pp. 4027–4032. https://doi.org/10.4229/25thEUPVSEC2010-4AV.3.20.

Sakakura, H., Itagaki, M., Sugiyama, M., 2016. Estimation of defect activation energy around pn interfaces of Cu (In, Ga) Se2 solar cells using impedance spectroscopy Estimation of defect activation energy around pn interfaces of Cu (In, Ga) Se 2 solar cells using impedance spectroscopy. Jpn. J. Appl. Phys. 012301.

Sharifi-Asl, S., Macdonald, D.D., 2014. Electrochemical Impedance Spectroscopy. Dev. Electrochem. Sci. Inspired by Martin Fleischmann 9781118694, 349–365. https://doi.org/10.1002/9781118694404.ch19.

Sopori, B., Basnyat, P., Devayajanam, S., Shet, S., Mehta, V., Binns, J., Appel, J., 2012. Understanding light-induced degradation of c-Si solar cells. Conf. Rec. IEEE Photovolt. Spec. Conf. 1115–1120. https://doi.org/10.1109/PVSC.2012.6317798.

Sopori, B., Zhang, Y., Chen, W., 1999. Process monitoring in solar cell manufacturing. In: 9th Work. Cryst. Silicon Sol. Cell Mater. Process. Breckenridge Color, pp. 1–10.

Suresh, M.S., 1996. Measurement of solar cell parameters using impedance spectroscopy. Sol. Energy Mater. Sol. Cells 43, 21–28. https://doi.org/10.1016/0927-0248(95)00153-0.

Tanahashi, T., Sakamoto, N., Shibata, H., Masuda, A., 2018. Localization and characterization of a degraded site in crystalline silicon photovoltaic cells exposed to acetic acid vapor. IEEE J. Photovolt. 8, 997–1004. https://doi.org/10.1109/JPHOTOV.2018.2839259.

Wills, R.H., Hall, F.E., Strong, S.J., Wohlgemuth, J.H., 1996. The AC photovoltaic module. In: Conf. Rec. Twenty Fifth IEEE Photovolt. Spec. Conf. pp. 1231–1234. https://doi.org/10.1109/pvsc.1996.564354.

Yadav, P., Pandey, K., Tripathi, B., Kumar, M., 2015a. Investigation of interface limited charge extraction and recombination in polycrystalline silicon solar cell: using DC and AC characterization techniques. Sol. Energy 116, 293–302. https://doi.org/10.1016/j.solener.2015.04.011.

Yadav, P., Tripathi, B., Pandey, K., Kumar, M., 2015b. Investigating the charge transport kinetics in poly-crystalline silicon solar cells for low-concentration illumination by impedance spectroscopy. Sol. Energy Mater. Sol. Cells 133, 105–112. https://doi.org/10.1016/j.solmat.2014.10.031.

Supplementary Information

Evaluation of impedance spectroscopy as a tool to characterize degradation mechanisms in silicon photovoltaics

Travis Yeow, Jing Sun, Zheng Yao, Jean-Nicolas Jaubert, Kevin P. Musselman*

*Email: kevin.musselman@uwaterloo.ca

Table S1: Current-voltage measurements of a (one) bifacial module before and after PID conditioning with simulated solar illumination on the front or backside.

State	V_{OC} (V)	I_{SC} (A)	V_{MP} (V)	I_{MP} (A)	Fill Factor	P_{MAX} (W)	% Decrease P_{MAX}
Front							
Initial	47.548	9.618	39.450	9.101	0.785	359.038	
After PID	46.646	9.400	38.575	8.740	0.769	337.148	6.1
Back							
Initial	46.893	7.102	39.477	6.782	0.804	267.716	
After PID	45.785	6.451	40.992	4.104	0.570	168.222	37.2

Table S2: Current-voltage measurements of a (one) PERC module under simulated solar illumination before and after CID conditioning

State	V_{OC} (V)	I_{SC} (A)	V_{MP} (V)	I_{MP} (A)	Fill Factor	P_{MAX} (W)	% Decrease P_{MAX}
Initial	39.192	9.602	32.616	9.105	0.789	296.958	
After CID	39.138	9.519	32.443	9.004	0.784	292.120	1.6

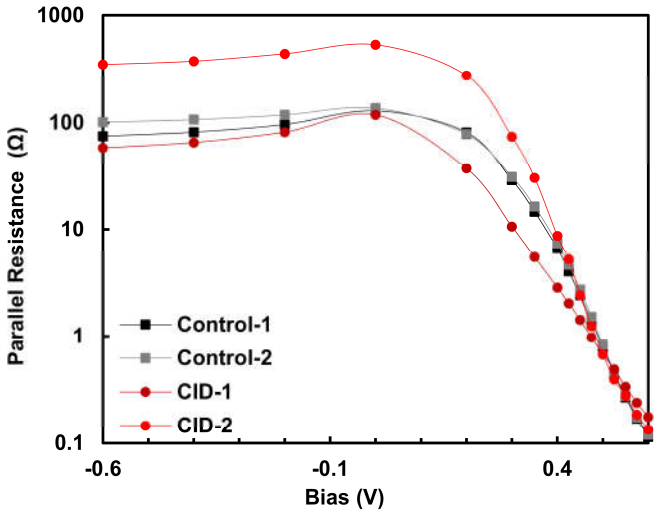

Figure S1: Parallel resistance as a function of bias voltage for 4 high quality silicon PERC cells (with no CIR). Two of the cells underwent CID conditioning and two did not. The parallel resistance was obtained by fitting the impedance spectra to an equivalent circuit with a series resistor, parallel resistor, and parallel capacitor.

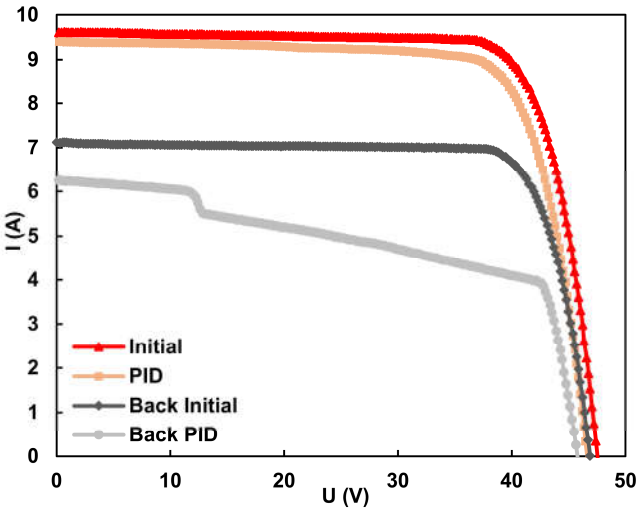

Figure S2: Current-voltage measurements of a bifacial module with and without PID, demonstrating a reduction in fill factor and short circuit current, particularly for backside illumination.